Mechanisms of damage formation in Eu-implanted GaN probed by X-ray diffraction

Bertrand Lacroix, Stéphanie Leclerc, Alain Declémy, Katharina Lorenz, Eduardo Alves, Pierre Ruterana

Mechanisms of damage formation in Eu-implanted GaN probed by X-ray diffraction

B. Lacroix[1] [(a)], S. Leclerc[1], A. Declémy[2], K. Lorenz[3], E. Alves[3] and P. Ruterana[1] [(b)]

[1] *CIMAP, UMR 6252 CNRS - ENSICAEN - CEA - UCBN, 6 Bd du Maréchal Juin, 14050 Caen cedex 4, France*
[2] *Institut Pprime, UPR 3346 CNRS - Université de Poitiers - ENSMA, Bd Marie et Pierre Curie, 86962 Futuroscope Chasseneuil cedex, France*
[3] *Instituto Tecnológico e Nuclear, Estrada Nacional 10, 2686-953 Sacavém, Portugal*

PACS 61.72.uj – Doping and ion implantation of III-V semiconductors
PACS 61.80.Jh – Ion radiation effects
PACS 61.05.C- – X-ray diffraction and scattering

Abstract –At low fluence, 300 keV Eu implantation in GaN leads to a strain increase followed by a saturation as observed by X-ray diffraction, while Rutherford backscattering/channeling remains insensitive to the radiation damage. Based on transmission electron microscopy, this saturation regime is attributed to a damaged region in the crystal bulk in which interaction between point defects and stacking faults (SFs) occurs, leading to the densification of the network of planar defects by the trapping of point defects. At higher fluences, above 2×10^{14} Eu/cm^2, the evolutions of strain state in another region and of the microstructure as observed by TEM indicate a modification of the degradation mechanisms which now involve a migration of point defects out of the region of SFs. This results in the formation of a highly strained area below the region of SFs made up of large point defect clusters, and in the extension of the SFs network towards the surface that eventually leads to its nanocrystallization.

Introduction. – Over the past years, rare earths (REs) doping of wide band-gap semiconductors has received a large interest due to expected promising applications in the field of optoelectronics and photonics [1–3]. The fabrication of white light-emitting devices requires the introduction of optically active REs elements above the solid solubility limit with a good control of their concentrations. In this context, ion implantation is an attractive technique that unfortunately generates structural damage degrading the properties of the materials. A good understanding of the damage formation during the implantation process is therefore required. Previous studies have pointed out a complex and non-conventional behavior of GaN under various implantation conditions, with a strong resistance to amorphization [4]. Following a Rutherford backscattering spectrometry analysis in the channeling geometry (RBS/C), Kucheyev et al. [5] reported a bimodal evolution of the damage taking place in the bulk and at the surface during implantation at room temperature (RT) and LN_2 temperature using light (^{12}C) and heavy (^{197}Au) ions at hundreds keV. The bulk damage has been

[(a)] E-mail: bertrand.lacroix@ensicaen.fr
[(b)] E-mail: pierre.ruterana@ensicaen.fr

related to the nucleation of a band of planar defects, whereas 'amorphization' was assumed to start at the surface. For REs implantation at 300 keV and RT, it was shown that the damage evolution of GaN is similar [6]. It proceeds through the generation, in the bulk, of prismatic and basal stacking faults (SFs) [7–9] growing laterally with the fluence, followed by the formation of a nanocrystalline layer at the surface [6]. The three types of basal stacking faults I_1, I_2 and E of the wurtzite structure ($\vec{R}_{I_1}=\frac{1}{6}<20\bar{2}3>$, $\vec{R}_{I_2}=\frac{1}{3}<10\bar{1}0>$, $\vec{R}_E=\frac{1}{2}<0001>$) were previously observed in the implanted region, with a clear predominance of the intrinsic I_1-type (around 90%) [6]. The nanocrystallization process was explained by the 'propagation' of the SFs network, thanks to the prismatic faults in the Drum ($\vec{R}_D=\frac{1}{2}<10\bar{1}1>$) and Amelinckx ($\vec{R}_A=\frac{1}{6}<20\bar{2}3>$) configurations, which breaks down mechanically when reaching the surface [10]. Nevertheless, up to now, the initial mechanism leading to the 'propagation' of planar defects towards the surface remains unclear, probably because the damage has been mainly measured using RBS/C which is mostly sensitive to the lattice disorder. In this work, we present an X-ray diffraction investigation to probe the evolution of the implantation induced strain.

Experiments. – GaN layers (2 μm-thick) were grown along the [0001] axis on a (0001) sapphire substrate by metal organic chemical vapor deposition. Channeled implantation along the *c*-axis with 300 keV Eu ions was performed at RT, over the fluence range from 5×10^{12} to 5×10^{15} Eu/cm^2. The estimated mean projected range of ions (Rp) from SRIM calculation [11] is 55 nm (without taking into account channeling and dynamic annealing effects). The implanted samples were studied by transmission electron microscopy (TEM), Rutherford backscattering spectrometry in channeling configuration (RBS/C) and X-ray diffraction (XRD). Cross-sections for TEM were thinned down to less than 10 μm by mechanical polishing, and then ion milled at low energy and LN_2 temperature. The post-implantation damage profiles were determined by RBS/C experiments using a 2 MeV He ion beam [12]. XRD measurements were performed on an automated laboratory-made two circles goniometer with the copper Kα_1 radiation (λ=1.5405 Å) provided by a 5 kW RIGAKU RU-200 generator with a vertical linear focus in combination with a quartz monochromator [13]. Symmetric θ-2θ scans were recorded around the (0004) Bragg reflection ($2\theta_B$=73.035 °) for which the penetration depth of X-rays in GaN (≈ 8 μm) is significantly larger than the extension of the implanted area. The strain along the surface normal (normal strain), ε_N, was directly determined by plotting the θ-2θ curves versus $q[0001]/H(0004)$, where $q[0001]$ is the component of the deviation vector along the surface normal [0001], from the reciprocal lattice vector $H(0004)$ of the (0004) planes [14].

Results and discussion. – Figure 1 shows θ-2θ scans around the (0004) reflection of GaN for different ion fluences. No modification of the (0004) peak is seen after implantation at 5×10^{12} Eu/cm^2 (not shown). At higher fluences, the intensity is scattered at negative $q[0001]/H(0004)$ values, indicating a dilatation of the lattice along the surface normal. At 5×10^{13} Eu/cm^2, a satellite peak is observed at ε_N=0.36%, and a progressive shift of this peak to ε_N=0.65% can be noticed when the fluence increases up to 2×10^{14} Eu/cm^2. The presence of a single and well-defined satellite peak may indicate that the implanted layer is quasi-homogeneously strained. Above 2×10^{14} Eu/cm^2, the scattered intensity distribution is clearly modified: a broadening is observed which points out a non-homogeneous normal strain profile. At the fluence of 3×10^{14} Eu/cm^2, this distribution extends from a peak at ε_N=0.6% to a maximum strain of about 0.8%. The position of the satellite peak at ε_N=0.6% remains unchanged above 3×10^{14} Eu/cm^2 which means that a saturation of the normal strain (S1) occurs in a localized region of the damaged area. At the same time, the maximum strain continuously increases with fluence. From 1×10^{15} Eu/cm^2, the X-ray scattered intensity decreases monotonically from the satellite peak at ε_N=0.6% to a maximum strain of approximately 1.6%, and there is no more evolution of the XRD curves which indicates a second saturation (S2) of the normal strain in the whole diffracting area.

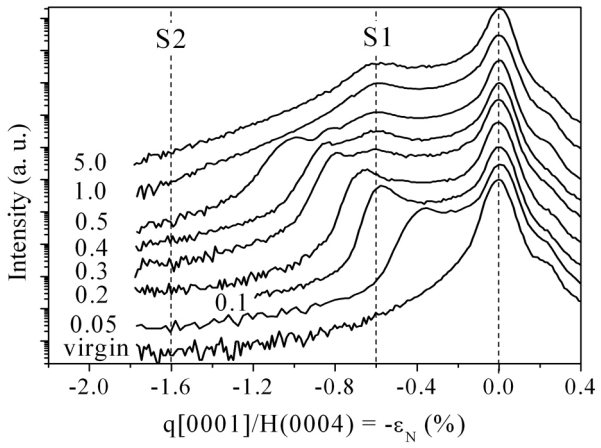

Fig. 1: θ-2θ scans performed around the (0004) reflection of GaN Eu-implanted at various fluences (indicated on the left of each curve and expressed in 10^{15} Eu/cm^2).

In order to understand the origin and the evolution of strain, XRD measurements have been compared with RBS/C and TEM results. In figure 2, the normal strain variations related to the satellite peak and to the maximum strain (figure 2(a)) are plotted with the damage kinetics in the bulk and at the surface (figure 2(b)) obtained from a previous RBS/C study [12]. Different regimes can be identified. In regime (*i*), below 2×10^{14} Eu/cm^2, the level of damage (RBS/C) remains low (< 0.05) and the normal strain (XRD) increases progressively. In this low fluence range, RBS/C appears almost insensitive to radiation damage whereas XRD shows significant lattice dilatations due to the formation of both point defect clusters and stacking faults in the implanted layer, as reported in a previous TEM investigation [6]. The next regime (*ii*), from 2×10^{14} to 1×10^{15} Eu/cm^2, is characterized by the first saturation of strain related to the satellite peak around 0.6% and the continuous increase of the maximum strain up to 1.6%. During this regime, bulk and surface damages increase slowly up to 5×10^{14} Eu/cm^2 and then rapidly. In regime (*iii*), from approximately 1×10^{15} to 2×10^{15} Eu/cm^2 and above, there is no more evolution of the normal strain. This strain saturation occurs at the same time as the saturation of the damage in the bulk part of the implanted area, whilst the surface damage still increases: such a behavior indicates that the surface does not contribute to the X-ray scattered intensity anymore. Then, in regime (*iv*), above 2×10^{15} Eu/cm^2, the surface damage level saturates at 0.9. This is consistent with the formation of the nanocrystalline layer at the surface around 2.5×10^{15} Eu/cm^2 [6].

As can be seen in the TEM micrographs of the 5×10^{14} Eu/cm^2 sample (figure 3), the damaged area, 190 nm in width, is composed of three layers (figure 3(a)) from which different strain states may arise: one layer of dark contrast (B), 80 nm in width, surrounded by two brighter layers, one of 40 nm at the surface (A), and another of more than 70 nm in the rear part (C). SFs and clusters of point defects are observed mainly in the B layer, as shown using the $\mathbf{g} = 1\bar{1}00$ and $\mathbf{g} = 0002$ dark field weak beam conditions, respectively (figure 3(b) and figure 3(c)). The C layer exhibits a concentration gradient of point defect clusters (observed as dark dots on figure 3(a)) which can explain the non-homogeneous strain distribution measured by XRD.

At high fluences in regime (*iv*), a similar three-layers structure is observed. As shown in figure 4 for the 3×10^{15} Eu/cm^2 implanted sample, the surface layer (A') is now nanocrystalline: obviously such a layer composed of misoriented nanograins cannot significantly contribute to the XRD signal which means that the two strain saturations arise only from the bulk (B and C layers). The C layer appears larger than before (> 100 nm) and contains point defect clusters in higher concentration especially close to the B/C interface (darker

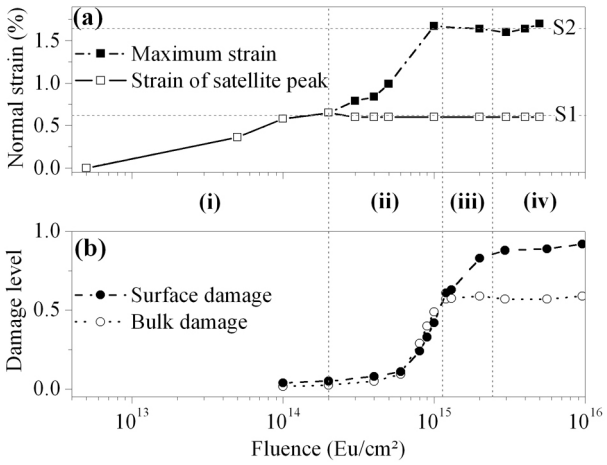

Fig. 2: Evolutions of the normal strain (determined by XRD) and damage level (determined by RBS/C) as a function of the ion fluence.

contrast). These observations indicate a migration of point defects towards the bulk and an increase of the cluster concentration explaining the broadening of the X-ray intensity distribution and the strain increase as the fluence increases. The presence of large clusters may also be responsible for the low scattered intensity due to a high static Debye-Waller factor [15]. As for the B layer, it is worth noticing that it still contains SFs, without any evolution in depth which shows that there is no 'propagation' of the SFs towards the bulk.

The results suggest that the normal strain saturation (S1) at 0.6% is localized in the B layer since this area is still present after implantation at high fluences. In this region,

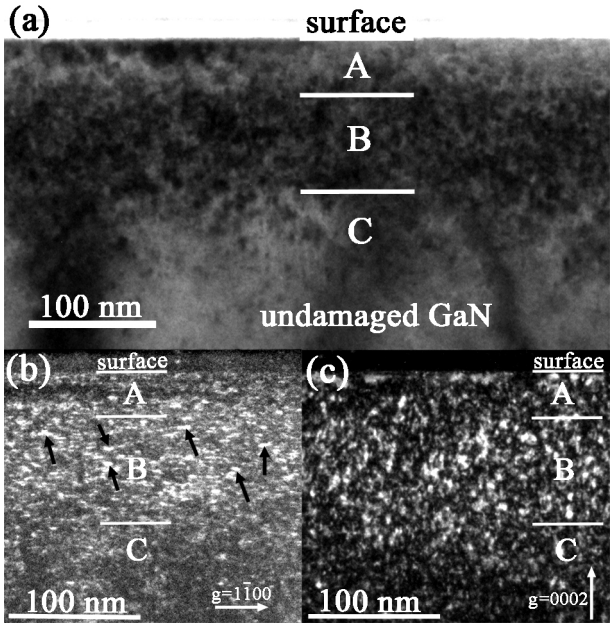

Fig. 3: TEM images of GaN implanted using 300 keV Eu ions with a fluence of 5×10^{14} Eu/cm^2. (a) Bright field along [11$\bar{2}$0]. Dark field using (b) $\mathbf{g} = 1\bar{1}00$ and (c) $\mathbf{g} = 0002$ weak beam conditions. On (b), the white lines parallel to the surface (indicated by arrows) correspond to basal SFs. On (c), the white dots correspond to point defect clusters.

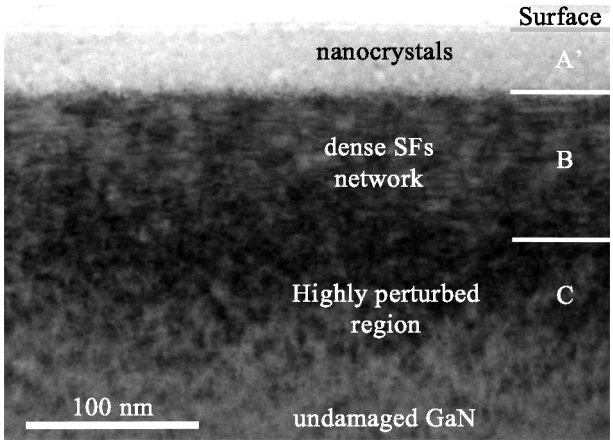

Fig. 4: Bright field TEM image (along $[11\bar{2}0]$) of GaN implanted using 300 keV Eu ions with a fluence of 3×10^{15} Eu/cm^2.

SFs and point defects coexist but it is difficult to separate their respective contributions to the strain state. Indeed, in contrast to point defects and clusters which are known to generate large hydrostatic distortions in the GaN network [16], the effect of SFs on the strain is not well known. However, we may assume that the contribution of SFs is not significant compared to point defects and clusters as their displacement vectors correspond to simple translations without change in atomic distances. Moreover, similarly to what has been reported concerning SiGe alloys [17, 18] or Si [19], the formation of extended defects in the B layer of GaN can be seen as an accommodation process of the damage to partially relax the strain. Here, it is obvious that the presence of SFs is necessary for the saturation of strain at 0.6% as the C layer which does not contain any SFs is subjected to much larger strains. The saturation S1 thus results from the interaction of point defects and clusters of point defects with SFs. Before the saturation S1, the SFs probably extend with the fluence by trapping point defects (in Si, it was shown that SFs can act as sinks for point defects [20]). At the same time, the concentration of point defects and clusters in the B layer that do not interact with SFs continues to increase which contributes to the increasing strain. The increasing density of point defects may enhance their recombination and trapping by the SFs. Some trapped point defects contribute to the extension and formation of BSFs and PSFs. The SFs are known to constitute preferential diffusion paths for point defects [21]. Thus, some point defects can migrate through the SF network towards the surface and the unperturbed bulk. As the density of SFs increases with connected PSFs and BSFs, the migration of point defects is enhanced which probably limits the concentration of point defects in the B layer in favour of the surface (A region) and the bulk C region. Beyond the strain saturation S1 (i. e. 2×10^{14} Eu/cm^2) point defects diffusing towards the surface could be trapped by smaller pre-existing SFs formed in the A layer, helping them to grow and inducing an extension of the SFs network towards the surface. In the C area which, in contrast to the A and B regions, is not subjected to the deposition of nuclear energy through dense collision cascades, SFs are not formed and point defects cannot be trapped: thus the strain cannot be minimized by the point defect interaction with SFs. Instead, point defects form large clusters giving rise to important strains in this region. The second strain saturation at 1.6% (S2) which coincides with the damage saturation in the bulk could be explained as follows. The nanocrystalline layer and the underlying SFs network may act as preferential diffusion paths towards the surface for the elimination of the point defects. This diffusion process towards the surface could be favored by the presence of large point defects clusters observed at the B/C interface which are likely to be non-mobile and which

may act as a barrier for the migration of defects towards the bulk, preventing any evolution of damage and strain distributions in the C layer.

As mentioned in the introduction, Eu doped GaN is a promising material for optoelectronic applications. However, the fabrication of efficient light emitting devices requires high temperature annealing [21] in order to optically activate the rare earth ions and to remove the implantation damage. It was shown earlier that the best results are obtained at temperatures around 1300°C [22]. However, the GaN surface needs to be capped as the material decomposes at temperature larger than 1000°C. Although optical activation of the present samples was achieved after annealing at 1000°C, close to complete structural recovery of the crystal at this temperature was only achieved for the lowest fluences ($< 5 \times 10^{14}$ Eu/cm^2) [12]. Furthermore, the nanocrystallization of the surface, observed on the TEM images beyond 3×10^{15} Eu/cm^2, has to be avoided because it would enhance the decomposition process during annealing. In this work, we pointed out that the formation of the surface nanocrystalline layer is the consequence of the enhancement of the defect migration towards the surface, which follows the saturation of strain S1 in the B region. Therefore, in order to avoid the diffusion of implantation induced-defects and to prevent the dissociation during the activation of rare earth ions, we suggest from the above results to perform a multi-step implantation/annealing procedure (as proposed in reference [23]), with the ion fluence of each implantation step limited to 1×10^{14} Eu/cm^2, i.e. before the implanted sample has reached the first strain saturation regime (S1).

Conclusion. – In summary, from the lowest fluences, an increase of strain along [0001] characterized by different saturation steps is observed. Around 2×10^{14} Eu/cm^2, a first saturation of the normal strain arising from an embedded region containing both point defects and stacking faults has been observed. The regime preceding this saturation is mainly related to an efficient trapping of point defects by the SFs, leading to the lateral extension of the planar defects. Then, as the SFs network becomes denser, an enhanced migration of point defects out of the embedded damaged region is expected. As suggested by XRD and TEM experiments, this migration results in the formation of a highly strained region beyond the SFs network due to point defect clustering and in the extension of the band of planar defects towards the surface that is responsible for the nanocristallization of the material. Finally, these results shed light on the possible mechanisms related to the 'efficient dynamic annealing' which has been put forward to account for the resistance of GaN to ion implantation damage.

* * *

This work has been supported by 'la Région Basse Normandie' and FCT Portugal (Ciência 2007, PTDC/CTM/100756/2008).

REFERENCES

[1] Steckl A. J. and Zavada J. M., *MRS Bull.*, **24** (1999) 9.
[2] Mamor M., Matias V., Vantomme A., Colder A., Marie P., and Ruterana P., *Appl. Phys. Lett.*, **85** (2004) 2244
[3] Park J. H. and Steckl A. J., *J. Appl. Phys.*, **98** (2005) 056108
[4] Williams J. S., *Mater. Sci. Eng. A*, **253** (1998) 8
[5] Kucheyev S. O., Williams J. S., Jagadish C., Zou J., and Li G., *Phys. Rev. B*, **62** (2000) 7510
[6] Gloux F., Wojtowicz T., Ruterana P., Lorenz K., and Alves E., *J. Appl. Phys.*, **100** (2006) 073520
[7] Potin V., Ruterana P. and Nouet G., *J. Phys. Condens. Matter*, **12** (2000) 10301
[8] Vermaut P., Nouet G., and Ruterana P., *Appl. Phys. Lett.*, **74** (1999) 694

[9] Ruterana P., Barbaray B., Béré A., Vermaut P., Hairie A., Paumier E., Nouet G., Salvador A., Botchkarev A. and Morkoc H., *Phys. Rev. B*, **59** (1999) 15917
[10] Ruterana P., Lacroix B. and Lorenz K., *J. Appl. Phys.*, **109** (2011) 013506
[11] Ziegler J. F., Biersack J. P., and Littmark U., *The Stopping and Range of Ions in Solids* (Pergamon, New York) 1985
[12] Lorenz K., Barradas N. P., Alves E., Rogan I. S., Nogales E., Martin R. W., O'Donnell K. P., Gloux F., and Ruterana P., *J. Phys. D: Appl. Phys.*, **42** (2009) 165103
[13] Leclerc S., Declémy A., Beaufort M. F., Tromas C. and Barbot J. F., *J. Appl. Phys.*, **98** (2005) 113506
[14] Debelle A., and Declémy A., *Nucl. Instrum. Methods Phys. Res.*, **268** (2010) 1460
[15] Leclerc S., Beaufort M. F., Declémy A., and Barbot J. F., *Appl. Phys. Lett.*, **93** (2008) 122101
[16] Kisielowski C., Krüger J., Ruvimov S., Suski T., Ager J. W., Jones E., Liliental-Weber Z., Rubin M., Weber E. R., Bremser M. D. and Davis R. F., *Phys. Rev. B.*, **54** (1996) 17745
[17] Cristiano F., Nejim A., Suprun-Belevich Yu, Claverie A., and Hemment P. L. F., *Nucl. Instrum. Methods Phys. Res. B*, **147** (1999) 35
[18] Vincent B., Damlencourt J.-F., Delaye V., Gassilloud R., and Clavelier L., *Appl. Phys. Lett.*, **90** (2007) 074101
[19] Zhou D. S., Holland O. W., and Budai J. D., *Appl. Phys. Lett.*, **63** (1993) 3580
[20] Antonelli A., Justo J. F., and Fazzio A., *Phys. Rev. B*, **60** (1999) 4711
[21] Kucheyev S. O., Williams J. S., and Pearton S. J., *Mater. Sci. Eng. R*, **33** (2001) 51
[22] ' Lorenz K., Wahl U., Alves E., Dalmasso S., Martin R. W., O'Donnell K. P., Ruffenach S. and Briot O., *Appl. Phys. Lett.*, **85** (2004) 2712
[23] Usov I. O., Koleske D. and Sickafus K. E., *Nucl. Instrum. Methods Phys. Res. B*, **267** (2009) 2962